Pulmonary Vascular Morphology Associated With Gas Exchange in Systemic Sclerosis Without Lung Fibrosis

Zhiwei Zhai, MSc, Marius Staring, PhD,* Maarten K. Ninaber, MD,† Jeska K. de Vries-Bouwstra, MD,‡ Anne A. Schouffoer, MD,‡ Lucia J. Kroft, MD,§ Jan Stolk, MD,† and Berend C. Stoel, PhD**

Purpose: Gas exchange in systemic sclerosis (SSc) is known to be affected by fibrotic changes in the pulmonary parenchyma. However, SSc patients without detectable fibrosis can still have impaired gas transfer. We aim to investigate whether pulmonary vascular changes could partly explain a reduction in gas transfer of SSc patients without fibrosis.

Materials and Methods: We selected 77 patients whose visual computed tomography (CT) scoring showed no fibrosis. Pulmonary vessels were detected automatically in CT images, and their local radii were calculated. The frequency of occurrence for each radius was calculated, and, from this radius histogram, 2 imaging biomarkers (α and β) were extracted, wherein α reflects the relative contribution of small vessels compared with large vessels, and β represents the vessel tree capacity. Correlations between imaging biomarkers and gas transfer [single-breath diffusion capacity for carbon monoxide corrected for hemoglobin concentration (DLCOc) %predicted] were evaluated with Spearman correlation. Multivariable stepwise linear regression was performed with DLCOc %predicted as the dependent variable and age, BMI, sPAP, FEV1 %predicted, TLC %predicted, FVC %predicted, α, β, voxel size, and CT-derived lung volume as independent variables.

Results: Both α and β were significantly correlated with gas transfer ($R = -0.29$, P-value $= 0.011$ and $R = 0.32$, P-value $= 0.004$, respectively). The multivariable stepwise linear regression analysis selected sPAP [coefficient $= -0.78$; 95% confidence interval (CI) $= -1.07$, -0.49; P-value < 0.001], β (coefficient $= 8.6$; 95% CI $= 4.07$, 13.1; P-value < 0.001), and FEV1% predicted (coefficient $= 0.3$; 95% CI $= 0.12$, 0.48; P-value $= 0.001$) as significant independent predictors of DLCOc %predicted ($R = 0.71$, P-value < 0.001).

Conclusions: In SSc patients without detectable pulmonary fibrosis, impaired gas exchange is associated with alterations in pulmonary vascular morphology.

Key Words: systemic sclerosis, pulmonary function tests, lung, helical computed tomography, computer-assisted image processing

(*J Thorac Imaging* 2019;34:373–379)

Systemic sclerosis (SSc) is an autoimmune connective tissue disease that involves multiple organs.[1] Pulmonary disease in SSc mainly consists of interstitial lung disease (ILD) and pulmonary hypertension (PH).[2] For evaluating severity of disease and response to treatment, pulmonary function tests (PFTs), such as diffusion capacity for carbon monoxide (DLCO) and forced vital capacity (FVC), are key outcome measures that play an important role as a surrogate for ILD and PH-related mortality.[3] In SSc-related ILD, structural changes of the lung parenchyma, that is, fibrosis, is known to affect PFTs.[2,4–7] In SSc-related PH, DLCO decreases years before diagnosis of PH.[8] Conversely, gas transfer can be mildly or moderately impaired in the absence of detectable pulmonary fibrosis and PH. As gas transfer studies measure the alveolar capillary membrane gas exchange efficiency,[9] we hypothesized that pulmonary vascular changes might partly explain this impaired DLCO, in the absence of pulmonary fibrosis.

Chest computed tomography (CT) is considered the most accurate noninvasive imaging method for pulmonary disease assessment.[10] Some studies on quantifying vascular tree morphology based on CT show promising performances for assessing pulmonary vascular disease.[11–16] Understanding the relation between vascular structure and pulmonary function may provide specific measurements for evaluating the response to treatment or for measuring the severity of pulmonary vascular disease. The aim of this study was to test whether vascular changes were related to impaired gas transfer in SSc patients without fibrosis. To this end, we developed an objective and automatic method to quantify the pulmonary vascular morphology and studied the association between these CT-derived imaging biomarkers and pulmonary function.

MATERIALS AND METHODS

Patients

We studied a cohort of 333 consecutive patients who had participated in our annual care program between April 2009 and October 2015.[17] The local Medical Ethical Committee approved the protocol, and all patients gave written informed consent for collection of clinical and diagnostic data contributing to the biobank of the Leiden Combined Care in SSc (CCIS) cohort. From this cohort, 83 patients had a chest CT scan wherein visual CT scoring showed no fibrosis and had PFTs measured within 8 days of the CT scan. Among these patients, image quality was insufficient for 6 patients to perform an accurate vascular analysis. Thus, 77 patients were selected for this study. On the basis of the degree of skin involvement, 3 subtypes of patients were classified: diffuse cutaneous SSc with skin involvement

From the Departments of *Radiology, Division of Image Processing; †Pulmonology; ‡Rheumatology; and §Radiology, Leiden University Medical Center, Leiden, The Netherlands.

Z.Z. is supported by China Scholarship Council scholarship No. 201406120046. The remaining authors declare no conflicts of interest.

Correspondence to: Berend C. Stoel, PhD, Department of Radiology, Division of Image Processing, Leiden University Medical Center, P.O. Box 9600, Leiden 2300 RC, The Netherlands (e-mail: b.c.stoel@lumc.nl).

Supplemental Digital Content is available for this article. Direct URL citations appear in the printed text and are provided in the HTML and PDF versions of this article on the journal's website, www.thoracicimaging.com.

DOI: 10.1097/RTI.0000000000000395

proximal to the elbows and knees; limited cutaneous SSc with skin involvement distal to the elbows and knees; and limited noncutaneous SSc without skin involvement.[18] The group consisted of 43 never-smokers, 31 ex-smokers, and 3 current smokers.

PFTs were performed under ERS/ATS guidelines,[19,20] including total lung capacity (TLC), FVC, forced expiratory volume in 1 second (FEV1), and single-breath diffusion capacity for carbon monoxide corrected for hemoglobin concentration (DLCOc). PFT results were expressed as a percentage of the predicted value (%predicted).[19,20] The DLCOc percentage of predicted (DLCOc %predicted) was selected as the key outcome measure of gas transfer.

The systolic pulmonary artery pressure (sPAP) was estimated using echocardiography with a commercially available system (Vingmed Vivd7; General Electric Vingmed Ultrasound, Milwaukee, WI). The sPAP was calculated from the tricuspid regurgitation peak gradient and the addition of right atrial pressure.[21] Patients with suspected PH (echocardiographic sPAP > 40 mm Hg) were tested by right heart catheterization (RHC). If the mean pulmonary artery pressure (mPAP) was > 25 mm Hg, the individual was diagnosed with PH.[22,23] Furthermore, the mPAP, cardiac output, pulmonary vascular resistance, and pulmonary artery wedge pressure were collected and used for determining the type of PH, under the 2015 ESC/ERS guidelines.[24] All patients were scanned with the same CT scanner (Aquilion 64; Toshiba Medical Systems, Otawara, Japan), with full inspiration and without contrast enhancement. The CT settings were as follows: tube voltage = 120 kV; tube current = 140 mA without modulation; rotation time = 0.4 s; collimation = 64×0.5 mm; helical beam pitch = 0.8; and the images were reconstructed with 0.5 mm slices.[25] Two observers (L.J.K. and A.A.S.), who were blinded to the patients' clinical information, scored the CT scans in consensus,[26] at 5 levels: (1) origin of the aortic arch branches; (2) main carina; (3) pulmonary venous confluence; (4) halfway between the third and fifth section; (5) immediately above the right hemidiaphragm. At each level, 6 variables were scored as percentages: total disease extent; proportion of ground glass; extent of reticular pattern; coarseness of reticular disease; extent of emphysema; and presence of bronchiectasis. Patients with 0% in all 30 variables were considered to have no parenchymal abnormalities. Patients involved in this study were without any suspicion for pulmonary veno-occlusive disease, as the CT scans did not show any signs of ground-glass opacities, septal thickening, or lymphadenopathy.

CT Analysis

For lung segmentation, we utilized multiatlas-based methods to flexibly capture anatomic variations using the Elastix registration toolbox.[27] Details on the atlas-based segmentation method can be found in the online supplements, Supplemental Digital Content 1 (http://links.lww.com/JTI/A114).

The final segmentation included both left and right lungs. Within each lung, the vascular trees were detected by a graph-cuts method,[28] wherein "vesselness" and CT intensity were combined into a single cost function. Previously, we evaluated this graph-cuts method using the public data set from VESSEL12[29] and obtained accurate vessel segmentation results.[30] 3D views of extracted pulmonary vascular trees are shown in Figures 1A–C. The entire vascular tree, that is, both arteries and veins, was automatically extracted and subsequently analyzed. In this automatic analysis, the distribution of the different radii of the entire vascular tree was quantified by first calculating the radius within each vessel, then a histogram from these data was constructed, and, finally, the shape of this histogram was analyzed, as detailed below.

At each location in the vascular tree, the radius was calculated by a skeletonization method (DtSkeletonization method of Mevislab 2.7[31]). This method selects voxels that are located at the center of a blood vessel by eroding the extracted vessels, and the corresponding radius is estimated by measuring the distance between the vessel boundary and the center. Examples of "skeletonized" vascular trees are shown in Figures 1D–F. Subsequently, the number of voxels in the vascular skeleton with a specific radius were counted, producing a histogram of the measured vascular radii. A logarithmic transformation was applied to the frequency of occurrence in order to obtain a linear relation between frequency and radius[32] (Figs. 1G–I). Thus, the index of each histogram bin represents the vessel radius, and the height of the bin represents the logarithm of the number of voxels with that specific radius. We used robust linear regression (robustfit method of MATLAB R2016b[33]) to analyze each radius histogram, and obtained 2 biomarkers (α, β) corresponding to the slope and intercept of the linear regression, respectively. The slope parameter α reflects the relative contribution of small vessels compared with large vessels (quantifying pruning of small vessels and dilatation of larger vessels), and the intercept β is related to the number of pulmonary capillaries estimated by extrapolation to radius 0, which reflects the vascular tree's capacity. To normalize for inspiration level and lung size, CT-derived lung volume was measured from the lung segmentations. As the vessel radius calculation might be affected by voxel size, the voxel size was also recorded for each patient.

Statistical Analysis

For patient characteristics, continuous variables were expressed as means with SD unless stated otherwise, and categorical variables were expressed as frequencies and percentages. Correlation between DLCOc %predicted or FVC %predicted and age, body mass index (BMI), sPAP, α, β, and CT-derived lung volume was expressed in terms of Spearman ρ correlation. Multivariable linear regression was used to determine independent predictors of DLCOc % predicted. DLCOc %predicted was entered as a dependent variable; age, BMI, sPAP, FEV1 %predicted, TLC %predicted, FVC %predicted α, β, voxel size, and CT-derived lung volume were used as independent variables. A stepwise method was used for selecting significant independent predictors. The same analyses were performed on the subgroup of patients without PH (n = 74), that is, by excluding the 3 patients with PH confirmed by RHC. All statistical analyses were performed by using SPSS (version 20.0.0; IBM Corp., Armonk, NY), and a 2-tailed *P*-value below 0.05 was considered statistically significant.

RESULTS

The patient characteristics are shown in Table 1. In this study, 77 patients (mean age, 49.9 ± 14.2, including 67 female individuals) were investigated, and the time difference between their CT and PFT is 1.19 ± 1.24 days. Among patients of this studied group, 3 patients were confirmed as having PH and were classified as pulmonary arterial

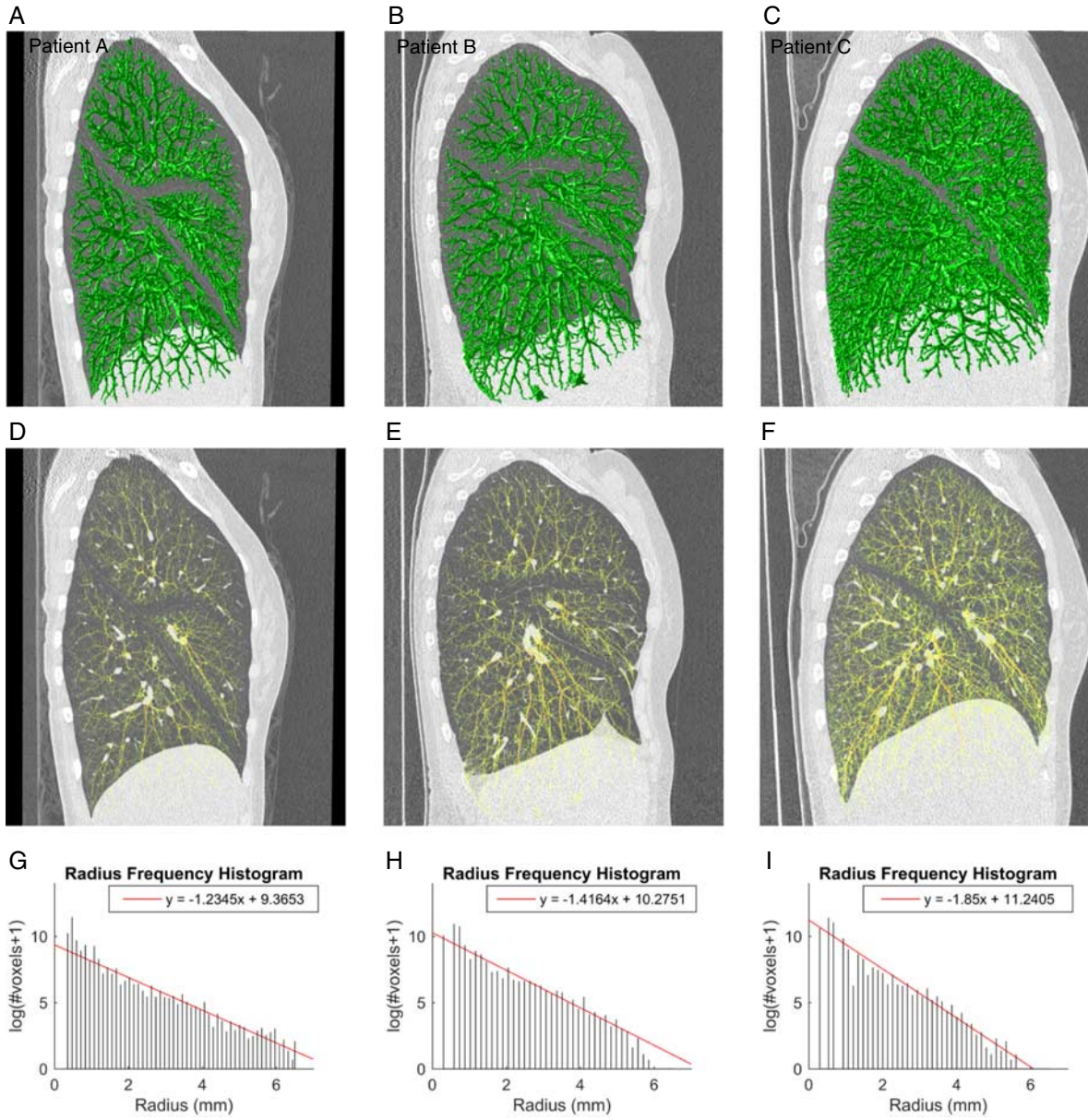

FIGURE 1. Three examples of vascular tree segmentation (A–C), vascular skeleton extraction from the corresponding vascular tree (D–F), and radius frequency histogram analysis of the vascular skeleton trees (G–I). Patients A, B, and C had a DLCOc of 46%, 69%, and 101.5% predicted, respectively, and lung volumes of 3.81, 6.2, and 4.23 L, respectively. The loss of vascular tree capacity, that is, a low intercept β and a flat slope α, is related to impaired gas transfer.

hypertension (group 1), according to their cardiac output, pulmonary vascular resistance, and pulmonary artery wedge pressure measurements. The average value of α and β were -1.44 ± 0.2 and 10.1 ± 0.62, respectively. Individually, age, α, β, and sPAP were moderately but significantly correlated with DLCOc %predicted, as presented in Table 2. The age and sPAP were significantly and negatively correlated with DLCOc %predicted. The biomarker α had a significant negative correlation with DLCOc %predicted ($R = -0.29$, P-value $= 0.011$), which implies that a less negative α (small-vessel pruning or large-vessel dilation) corresponds to a more impaired gas exchange (lower DLCOc %predicted). β had a positive significant correlation with DLCOc % predicted ($R = 0.32$, P-value $= 0.004$), which implies that a lower β (a low capacity of the vascular tree) corresponds to a more impaired gas exchange. The corresponding scatter plots are presented in Figure 2.

The results of the multivariable stepwise linear regression analysis for DLCOc %predicted as dependent variable are shown in Table 3. The multivariable stepwise regression analysis selected sPAP (coefficient $= -0.78$; 95% confidence interval [CI] $= -1.07$, -0.49; P-value < 0.001), β (coefficient $= 8.6$; 95% CI $= 4.07$, 13.12; P-value < 0.001), and FEV1 %predicted (coefficient $= 0.3$; 95% CI $= 0.12$, 0.48; P-value $= 0.001$) as significant and independent predictors of DLCOc %predicted ($R = 0.71$, P-value < 0.001). By

TABLE 1. Patient Group Characteristics

No. subjects	77
Female (n [%])	67 (87)
Age (y)	49.9 ± 14.2
BMI (kg/m^2)	24.6 ± 5.24
sPAP (mm Hg) (n = 77)	26.9 ± 10.4
mPAP (mm Hg) (n = 3)	40.3 ± 11
CO (L/min) (n = 3)	5.17 ± 0.9
PVR (dyn s/cm^5) (n = 3)	405.3 ± 149
PAWP (mm Hg) (n = 3)	11 ± 2.6
MRSS	3.38 ± 4.28
Type of SSc (n [%])	
DcSSc	8 (10.4)
LcSSc	51 (66.2)
LSSc	18 (23.4)
Autoantibodies (n [%])	
ANA	74 (96.1)
Anti-Scl-70*	4 (4.2)
Anticentromere†	53 (68.8)
RNA polymerase III	1 (1.3)
Pulmonary function (%predicted)	
DLCOc	70.4 ± 16.7
FVC	107 ± 17.4
FEV1	98.9 ± 16.8
TLC	95.7 ± 12.2
CT-derived measurements	
α	−1.44 ± 0.2
β	10.1 ± 0.62
Lung volume (L)	4.73 ± 1.24

*One patient with doubtful Anti-Scl-70.
†One patient with missing data.
ANA indicates antinuclear antibody; Anti-Scl-70, anti-topoisomerase; DcSSc, diffuse cutaneous SSc; DLCOc, single-breath diffusion capacity for carbon monoxide corrected with the haemoglobin concentration; FVC, forced vital capacity; LcSSC, limited cutaneous SSc; LSSC, limited noncutaneous SSc; PVR, pulmonary vascular resistance; sPAP, systolic pulmonary arterial pressure, obtained from echocardiography; TLC, total lung capacity.

including β in the model, an additional 10% of variation in gas transfer could be explained (from $R = 0.56$ to $R = 0.66$).

For additional analysis, we evaluated the relationships between imaging biomarkers and pulmonary ventilation, that is, FVC %predicted. As presented in Table 2, the correlation between age, BMI, sPAP, α, β, and FVC % predicted was not significant, whereas CT-derived lung volume was significantly correlated with FVC %predicted ($R = 0.41$, P-value < 0.001). Furthermore, the correlations between image biomarkers and sPAP were investigated. The correlation between sPAP and BMI ($R = 0.05$, P-value $= 0.676$), α ($R = 0.08$, P-value $= 0.509$), β ($R = -0.01$, P-value $= 0.92$), and lung volume ($R = -0.11$, P-value $= 0.333$) were not significant, whereas age had a significant correlation with sPAP ($R = 0.53$, P-value < 0.001). In the statistical analyses on the subgroup of patients without PH (n = 74), α ($R = -0.34$, P-value $= 0.003$) and β ($R = 0.42$, P-value < 0.001) were significantly correlated with DLCOc %predicted; β was the first selected independent predictor of DLCOc %predicted, followed by sPAP and FEV1 %predicted, in multivariable stepwise regression. The results of the subgroup analyses are shown in the online supplements, Supplemental Digital Content 1 (http://links.lww.com/JTI/A114).

TABLE 2. Correlations, *R* (*P*-value), Between CT Imaging Biomarkers and PFTs

	DLCOc %Predicted	FVC %Predicted
α	−0.29 (0.011)	−0.14 (0.243)
β	0.32 (0.004)	0.15 (0.187)
sPAP	−0.38 (0.001)	−0.01 (0.909)
BMI	0.19 (0.105)	0.26 (0.023)
Age (y)	−0.29 (0.01)	0.14 (0.23)
Lung volume	0.18 (0.12)	0.41 (<0.001)

DISCUSSION

We studied the pulmonary vascular morphology among SSc patients without pulmonary fibrosis. An automatic method was applied to CT images (without contrast medium), for characterizing the pulmonary vasculature by quantifying the vascular system with a radius histogram analysis. To our knowledge, this is the first report on the relationship between pulmonary vascular tree capacity (the number of pulmonary capillaries estimated from CT) and gas transfer. Two CT-derived imaging biomarkers were introduced that are significantly correlated with DLCOc % predicted, demonstrating that gas transfer is associated with changes in vascular morphology. This may be useful in understanding the pathophysiology of this subgroup of SSc patients whose gas transfer deteriorates in the course of their disease without detectable pulmonary fibrosis.

Pulmonary vasculature was quantitatively assessed by two measurements, α and β. Biomarker α, the histogram slope, reflects the relative contribution of small vessels compared with large vessels, quantifying pruning of distal vessels and dilatation of the proximal vessels. Biomarker β, the histogram intercept, is estimated by extrapolation to radius 0, which provides an estimate of the vascular tree capacity, without actually detecting pulmonary capillaries. The biomarker α was significantly correlated with biomarker β ($R = -0.91$, P-value < 0.001), implying that the reduction of vascular tree capacity could result in a change in the relative contribution of small vessels compared with large vessels. sPAP, β, and FEV1 %predicted were selected by the stepwise method, whereas α, was excluded, as it did not explain additional DLCOc %predicted variation, probably due to the high correlation between α and β. To illustrate the effect of α and β (pruning/dilatation and vascular tree capacity), the cases of 3 patients are discussed in more detail (Figs. 1, 2). Patient A with a low DLCOc %predicted obtained a flat slope α and a low intercept β, indicating vessel pruning/dilatation and a loss of vascular tree capacity, as compared with the other patients. This was confirmed by visual inspection of the vascular tree in Figure 1. Compared with patient B who had a moderate DLCOc %predicted, α, and β, patient C had a higher DLCOc %predicted, lower α value, and higher β value, which implied that a better gas transfer corresponds to a lower vessel pruning/dilatation and higher vascular tree capacity. As the studied patient group consisted of SSc patients without pulmonary fibrosis, CT-derived lung volume was considered to reflect the TLC. As the voxel size might affect the vascular morphology measurements, voxel size was entered as the independent variable in the multivariable linear regression. It proved, however, to be a nonsignificant factor in predicting gas transfer.

DLCOc %predicted and FEV1 %predicted correlated significantly in our study population ($R = 0.4$, P-value = 0.001). In the multivariable linear regression, the FEV1% predicted was a significant independent predictor of DLCOc %predicted, which implies that pulmonary gas transfer was associated with pulmonary ventilation (air flow). The sPAP had a negative and significant correlation with DLCOc % predicted, and the sPAP was a significant predictor of

Copyright © 2019 Wolters Kluwer Health, Inc. All rights reserved.

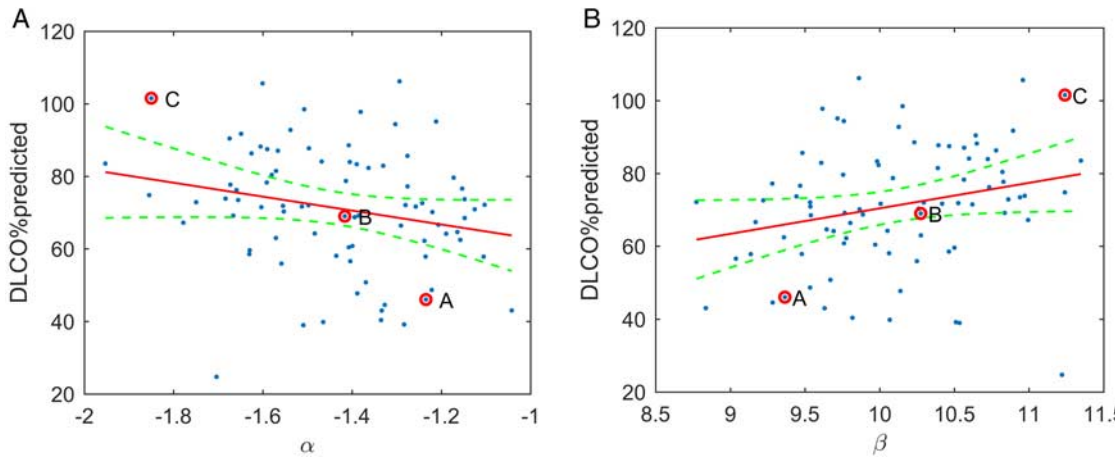

FIGURE 2. Correlation between imaging biomarkers and lung function (A, B, and C are corresponding to patients A, B, and C in Fig. 1, respectively). A, Correlation between α and DLCOc %predicted ($R = -0.29$, P-value = 0.011). B, Correlation between β and DLCOc %predicted ($R = 0.32$, P-value = 0.004).

DLCOc %predicted in the multivariable linear regression, which indicates that pulmonary pressure (blood flow) could affect gas transfer. In the subgroup of patients without PH, the performance of the biomarkers in predicting gas transfer was similar to those of the whole patient group, which implies that excluding or including these 3 PH patients did not change the validity of the biomarkers.

Several aspects of the correlation between β and DLCOc %predicted as well as the influence of FVC require some clarification. The correlation between DLCOc %predicted and β may be influenced by the position of the patient in both measurements (ie, the sitting position during gas transfer studies and the supine position during chest CT). Two determinants of DLCO, membrane diffusing capacity (Dm) and capillary blood volume (Vc), have been known to be affected by posture and gravity. A postural change from the sitting to the supine position in normal gravity, wherein some degree of heterogeneity between the dependent and nondependent lung region persists, can result in an increase in Vc and not Dm, and an overall increase in DLCO up to 15%.[9,34] Therefore, it seems plausible that this could have weakened the correlation between β and DLCOc %predicted. Furthermore, as α and β have not been evaluated in normal subjects, values between the "upper and lower limit of normal" of α and β may exist in our study population. This may be another factor that could have led to weakening the correlation between β and DLCOc %predicted. However, the protection of healthy individuals against radiation exposure prevents us from prospectively measuring α and β in CT images from normal controls, and retrospectively collecting negative CT examinations generally lacks confirmation by PFTs; these CT scans are usually contrast enhanced, affecting the vascular morphology analysis.

Currently, studies on quantifying vascular tree morphology with CT imaging also showed promising results for assessing pulmonary vascular pathology associated with other pulmonary diseases. In chronic obstructive pulmonary disease related studies,[11,12] the pulmonary vessel morphology was quantified using CT scans without contrast as the percentage of small vessels, that is, vessels with cross-section area (CSA) $<5\ mm^2$ (%CSA $< 5\ mm^2$). The quantification had a weak but significant correlation with PFTs[11] and a significant negative correlation with mPAP.[12] Furthermore, smoking-related chronic obstructive pulmonary disease is characterized by distal pruning of the small vessels, which was assessed with the ratio between small vessel volume with CSA $< 5\ mm^2$ and total blood vessel volume (BV5/TBV).[13] In one PH study,[14] pulmonary vascular morphology was quantified with contrast-enhanced chest CT in 24 patients (18 with and 6 without PH). Vascular remodelling characterized by vessel tortuosity and 3D fractal dimensions correlated significantly with RHC measurements. Furthermore, in chronic thromboembolic PH, the disease was quantified as pulmonary morphologic changes with CT scans,[15] including pruning of the distal vessel and dilation of the proximal vessels, which were measured with the ratio BV5/TBV and the ratio BV > 10/TBV (where BV > 10 is the blood volume for all vessels with a CSA $> 10\ mm^2$), respectively. These biomarkers differed significantly between chronic thromboembolic PH patients and control individuals, and they correlated with RHC measures. In this study, quantification on portions of pulmonary vascular system based on CSA or quantification of the pulmonary vascular fractal dimension was performed. In our study, however, we considered the pulmonary vessels as a continuous system, by quantifying vascular changes including all vessel radii by histogram analysis, instead of analyzing only parts of the vascular tree. This yielded 2 biomarkers, α and β, that characterized the vascular tree in a more global approach, showing an association with gas transfer.

TABLE 3. Multivariable Stepwise Linear Regression Analysis for DLCOc %Predicted (n = 77)

	Multivariable Regression	
Parameter	**Regression Coefficient [95% CI]**	***P***
Age (y)	—	—
BMI	—	—
sPAP	−0.78 [−1.07, −0.49]	< 0.001
FVC %predicted	—	—
FEV1 %predicted	0.3 [0.12, 0.48]	0.001
TLC %predicted	—	—
α	—	—
β	8.6 [4.07, 13.1]	< 0.001
Voxel size	—	—
Lung volume	—	—

There are some limitations in our analysis. The automatic method used in the present study could not distinguish arteries from veins. As vascular changes may differ between arteries and veins, improved correlation may be expected with arteries evaluated separately from veins. However, even without this distinction, we already found a significant association with gas transfer. Furthermore, we assessed both lungs together for each patient. More specific analysis of separate lungs or lung lobes may provide a more localized assessment of vascular changes. All patients in this study were scanned by the same scanner; thus, when adopting the automatic method to other CT scanners, the parameters for vessel extraction might need to be adjusted. The studied group only included SSc patients without a control group. Data on normal vasculature morphology of healthy people would enhance our understanding. Nevertheless, our method was still able to detect variances in the pulmonary vasculature. Because of a lack of pathology specimens in these SSc patients, validation of the imaging measurements against pathology was not possible. In the future, we aim to prospectively follow-up changes in the pulmonary vascular morphology in these patients over time, and evaluate whether these subtle changes precede functional changes in pulmonary testing. Studying the morphologic changes of pulmonary vasculature in the patients with PH-related diseases, such as chronic thromboembolic PH, is also an interesting point of our future work, as the metric of morphologic changes could help to predict an early development or monitor effects of treatment.

In conclusion, we characterized the pulmonary vasculature by 2 CT-derived imaging biomarkers from vascular radius analysis. These 2 imaging biomarkers, indicating small-vessel pruning/large-vessel dilation and loss of vascular tree's capacity, are associated with decreased gas transfer in the studied SSc patient group. The method may help understand the relationship between pulmonary vascular changes in SSc and lung function, in the absence of detectable fibrosis.

REFERENCES

1. Hinchcliff M, Varga J. Systemic sclerosis/scleroderma: a treatable multisystem disease. *Am Fam Physician*. 2008;78:961–968.
2. Cappelli S, Randone SB, Camiciottoli G, et al. Interstitial lung disease in systemic sclerosis: where do we stand? *Eur Respir Rev*. 2015;24:411–419.
3. Goh NS, Hoyles RK, Denton CP, et al. Short term pulmonary function trends are predictive of mortality in interstitial lung disease associated with systemic sclerosis. *Arthritis Rheumatol*. 2017;69:1670–1678.
4. Bussone G, Mouthon L. Interstitial lung disease in systemic sclerosis. *Autoimmun Rev*. 2011;10:248–255.
5. Herzog EL, Mathur A, Tager AM, et al. Review: interstitial lung disease associated with systemic sclerosis and idiopathic pulmonary fibrosis: how similar and distinct? *Arthritis Rheumatol*. 2014;66:1967–1978.
6. Manners D, Wong P, Murray C, et al. Correlation of ultra-low dose chest CT findings with physiologic measures of asbestosis. *Eur Radiol*. 2017;27:3485–3490.
7. Kim HJ, Brown MS, Elashoff R, et al. Quantitative texture-based assessment of one-year changes in fibrotic reticular patterns on HRCT in scleroderma lung disease treated with oral cyclophosphamide. *Eur Radiol*. 2011;21:2455–2465.
8. Mukerjee D, George DS, Knight C, et al. Echocardiography and pulmonary function as screening tests for pulmonary arterial hypertension in systemic sclerosis. *Rheumatology*. 2004;43:461–466.
9. West J. *Respiratory Physiology The Essentials*. Philadelphia, PA, Baltimore, MD, New York, NY, London, Buenos Aires, Hong Kong, Sydney, Tokyo: Lippincott Williams & Wilkins; 2000.
10. Martin SG, Kronek L-P, Valeyre D, et al. High-resolution computed tomography to differentiate chronic diffuse interstitial lung diseases with predominant ground-glass pattern using logical analysis of data. *Eur Radiol*. 2010;20:1297–1310.
11. Matsuoka S, Washko GR, Dransfield MT, et al. Quantitative CT measurement of cross-sectional area of small pulmonary vessel in COPD: correlations with emphysema and airflow limitation. *Acad Radiol*. 2010;17:93–99.
12. Matsuoka S, Washko GR, Yamashiro T, et al. Pulmonary hypertension and computed tomography measurement of small pulmonary vessels in severe emphysema. *Am J Respir Crit Care Med*. 2010;181:218–225.
13. Estépar RSJ, Kinney GL, Black-Shinn JL, et al. Computed tomographic measures of pulmonary vascular morphology in smokers and their clinical implications. *Am J Respir Crit Care Med*. 2013;188:231–239.
14. Helmberger M, Pienn M, Urschler M, et al. Quantification of tortuosity and fractal dimension of the lung vessels in pulmonary hypertension patients. *PLoS One*. 2014;9:e87515.
15. Rahaghi F, Ross J, Agarwal M, et al. Pulmonary vascular morphology as an imaging biomarker in chronic thromboembolic pulmonary hypertension. *Pulm Circ*. 2016;6:70–81.
16. Coste F, Dournes G, Dromer C, et al. CT evaluation of small pulmonary vessels area in patients with COPD with severe pulmonary hypertension. *Thorax*. 2016;71:830–837.
17. Meijs J, Schouffoer AA, Marsan NA, et al. Therapeutic and diagnostic outcomes of a standardised, comprehensive care pathway for patients with systemic sclerosis. *RMD Open*. 2016;2:e000159.
18. Meijs J, Schouffoer AA, Marsan NA, et al. A prediction model for progressive disease in systemic sclerosis. *RMD Open*. 2015;1:e000113.
19. Graham BL, Brusasco V, Burgos F, et al. 2017 ERS/ATS standards for single-breath carbon monoxide uptake in the lung. *Eur Respir J*. 2017;49:1600016.
20. Miller MR, Hankinson J, Brusasco V, et al. Standardisation of spirometry. *Eur Respir J*. 2005;26:319–338.
21. Kircher BJ, Himelman RB, Schiller NB. Noninvasive estimation of right atrial pressure from the inspiratory collapse of the inferior vena cava. *Am J Cardiol*. 1990;66:493–496.
22. Yiu KH, Ninaber MK, Kroft LJ, et al. Impact of pulmonary fibrosis and elevated pulmonary pressures on right ventricular function in patients with systemic sclerosis. *Rheumatology*. 2015;55:504–512.
23. Bakker ME, Ninaber MK, Stolk J, et al. Lung density and pulmonary artery diameter are predictors of pulmonary hypertension in systemic sclerosis. *J Thorac Imaging*. 2017;32:391–397.
24. Galiè N, Humbert M, Vachiery J-L, et al. 2015 ESC/ERS Guidelines for the diagnosis and treatment of pulmonary hypertension. The Joint Task Force for the Diagnosis and Treatment of Pulmonary Hypertension of the European Society of Cardiology (ESC) and the European Respiratory Society (ERS): endorsed by: Association for European Paediatric and Congenital Cardiology (AEPC), International Society for Heart and Lung Transplantation (ISHLT). *Eur Heart J*. 2016;37:67–119.
25. Ninaber MK, Stolk J, Smit J, et al. Lung structure and function relation in systemic sclerosis: application of lung densitometry. *Eur J Radiol*. 2015;84:975–979.
26. Goh NS, Desai SR, Veeraraghavan S, et al. Interstitial lung disease in systemic sclerosis: a simple staging system. *Am J Respir Crit Care Med*. 2008;177:1248–1254.
27. Klein S, Staring M, Murphy K, et al. Elastix: a toolbox for intensity-based medical image registration. *IEEE Trans Med Imaging*. 2010;29:196–205.
28. Boykov Y, Kolmogorov V. An experimental comparison of min-cut/max-flow algorithms for energy minimization in vision. *IEEE Trans Pattern Anal Mach Intell*. 2004;26:1124–1137.
29. Rudyanto RD, Kerkstra S, Van Rikxoort EM, et al. Comparing algorithms for automated vessel segmentation in computed

tomography scans of the lung: the VESSEL12 study. *Med Image Anal*. 2014;18:1217–1232.
30. Zhai Z, Staring M, Stoel BC. Lung vessel segmentation in CT images using graph cutsSPIE Medical Imaging. *Int Soc Optics Photonics*. 2016;97848:97842K.
31. Selle D, Preim B, Schenk A, et al. Analysis of vasculature for liver surgical planning. *IEEE Trans Med Imaging*. 2002;21: 1344–1357.
32. O'Dell WG, Govindarajan ST, Salgia A, et al. Traversing and labeling interconnected vascular tree structures from 3D medical imagesSPIE Medical Imaging. *Int Soc Optics Photonics*. 2014;90315:90343C.
33. Dumouchel W, O'Brien F. Integrating a robust option into a multiple regression computing environment. In: Buja A, Tukey PA, eds. Computing and graphics in statistics. *Institute for Mathematics and Its Applications*. New York: Springer-Verlag; 1992:41–48.
34. Terzano C, Conti V, Petroianni A, et al. Effect of postural variations on carbon monoxide diffusing capacity in healthy subjects and patients with chronic obstructive pulmonary disease. *Respiration*. 2009;77:51–57.